ACS APPLIED ENERGY MATERIALS
Cite This: ACS Appl. Energy Mater. 2019, 2, 8946−8955
Article
www.acsaem.org

Ion Exchange Synthesis of Cobalt Ion Modified Titanate Nanoarray as an Electrocatalyst toward Efficient Hydrogen Evolution Reaction

Hongfang Du,[†,‡,∥] Zhi Liang Zhao,[†,∥] Lian Ying Zhang,[†,∥] Yubin Niu,[†,∥] Ting Yu,*[,‡] and Chang Ming Li*[,†,§,∥,⊥]

[†]Institute for Clean Energy and Advanced Materials, Southwest University, Chongqing 400715, People's Republic of China
[‡]Division of Physics and Applied Physics, School of Physical and Mathematical Sciences, Nanyang Technological University, 637371, Singapore
[§]Institute of Materials Science and Devices, Suzhou University of Science and Technology, Suzhou 215011, People's Republic of China
[∥]Chongqing Key Laboratory for Advanced Materials and Technologies of Clean Energies, Chongqing 400715, People's Republic of China
[⊥]Institute of Advanced Cross-Field Science and College of Life Science, Qingdao University, Qingdao 200671, People's Republic of China

Supporting Information

ABSTRACT: Cobalt ion modified titanate nanoarray (CTO NA) with a three-dimensional hierarchical structure is synthesized via a facile ion exchange strategy and further developed as an electrocatalyst toward efficient hydrogen evolution reaction (HER). In 0.1 M KOH solution, CTO NA exhibits a low Tafel slope of 93 mV dec^{-1} and a small overpotential of 199 mV at a current density of 10 mA cm^{-2} as well as high electrochemical stability for HER. The superior electrocatalytic performance of CTO NA is attributed to the unique chemical composition and layered crystal structure for improved electrode kinetics. Meanwhile, the three-dimensional hierarchical morphology of CTO NA also contributes to fast charge transfer and greatly enhanced mass transport in electrochemical reaction. This work holds a great promise for the as-prepared CTO NA to be an alternative for the noble metals based catalysts toward large scale hydrogen production via water electrolysis.

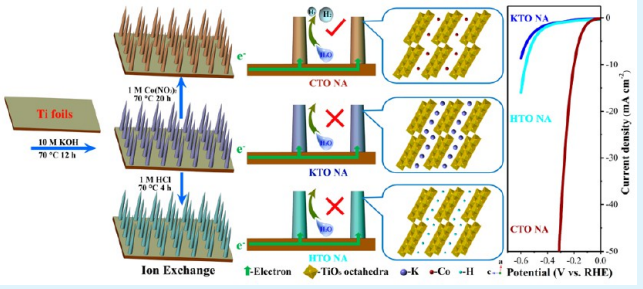

KEYWORDS: *hydrogen evolution reaction, cobalt titanate, nanoarray, electrocatalyst, alkali metal titanate*

1. INTRODUCTION

Hydrogen is considered as a clean and renewable energy source to address the global issues of energy shortage and environmental pollution stemming from the overconsumption of fossil fuels.[1−4] Currently, hydrogen is mainly produced by high-temperature steam re-forming method which greatly suffers from contamination and harsh operating conditions.[5,6] Water, consisting of hydrogen and oxygen elements, is one of the most abundant sources on the earth; hydrogen evolution from water is thus considered as a promising way to generate hydrogen energy.[7,8] Electrolysis of water is a convenient way to convert water to highly pure hydrogen due to the facile electrical energy transport and simple equipment requirements.[2] However, the mass production of hydrogen via water electrolysis is seriously hindered by the sluggish electrode kinetics of cathodic hydrogen evolution reaction (HER).[9,10] Consequently, noble metal based materials (such as Pt) are employed as efficient electrocatalysts to facilitate the electrode kinetics of HER, but the nobles are globally scarce and highly expensive which impede their broad application.[11] Therefore, there is an urgent need to develop inexpensive electrocatalysts for HER while keeping the catalytic activity comparable to that of nobles.[12]

Numerous research efforts have been devoted to this area, and various noble metal free materials are identified to have HER activity.[13] Among the large number of active materials, layered compounds have become an extremely attractive research topic due to their unique crystal structure and great potential in practical applications.[1] Alkali metal titanates, a class of materials comprising TiO_6 octahedral units and alkali ions, have intriguing physicochemical properties, among which $K_2Ti_4O_9$ with a layered crystal structure has been intensively investigated.[14,15] In $K_2Ti_4O_9$, each TiO_6 octahedron shares edges with its neighbors to form a negatively charged layer, and the interlayer regions are occupied with positively charged K^+.[16] The layered crystal structure of $K_2Ti_4O_9$ offers the

Received: October 9, 2019
Accepted: November 19, 2019
Published: November 19, 2019

Downloaded via NANYANG TECHNOLOGICAL UNIV on April 10, 2021 at 12:56:18 (UTC).
See https://pubs.acs.org/sharingguidelines for options on how to legitimately share published articles.

© 2019 American Chemical Society

DOI: 10.1021/acsaem.9b01994
ACS Appl. Energy Mater. 2019, 2, 8946−8955

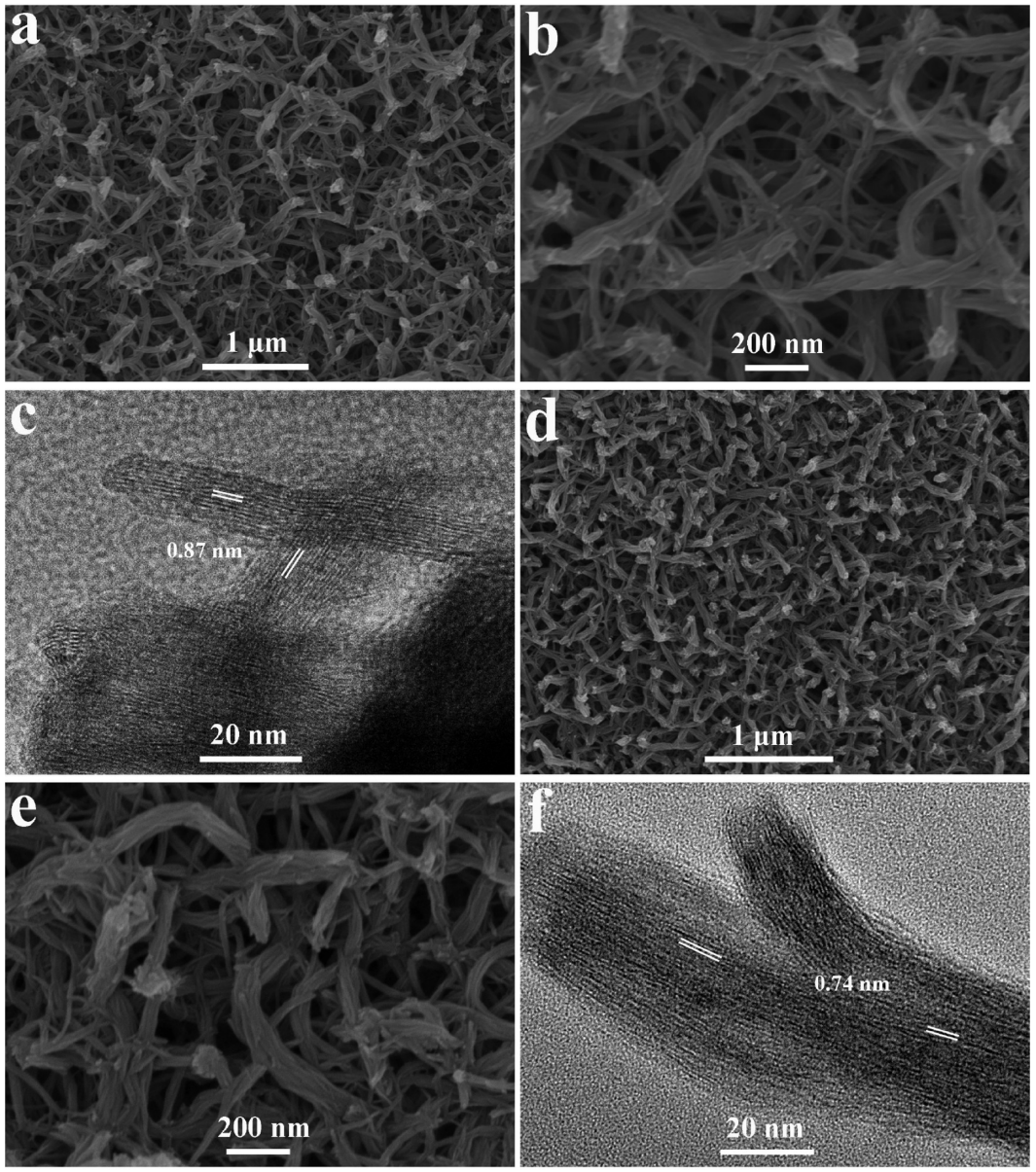

Figure 1. (a) Low- and (b) high-magnification SEM images and (c) high-resolution TEM image of KTO NA; (d) low- and (e) high-magnification SEM images and (f) high-resolution TEM image of CTO NA.

possibility of ionic conduction and ion exchange along the layers.[16] Actually, $K_2Ti_4O_9$ has strong ion exchange capability which allows protons,[17] metal ions,[18] and organic molecules,[19] etc., to replace the alkali ions. As a result, $K_2Ti_4O_9$ has extensively been studied as adsorbents to remove toxic heavy metal ions from aqueous solutions.[20] Besides, $K_2Ti_4O_9$ and its derivatives also have been investigated as electrode materials for battery and photocatalysis.[21,22] In view of its favorable crystal structure and tunable chemical composition, $K_2Ti_4O_9$ and its derivatives would be good candidates as high-performance electrocatalysts toward HER. However, to the best of our knowledge, the HER catalytic behaviors of alkali metal titanate based materials have not been explored so far.

In this work, potassium titanate nanoarray (KTO NA, $K_2Ti_4O_9$) with a three-dimensional hierarchical structure was in situ grown on Ti foil in a concentrated KOH solution. Cobalt ion modified titanate nanoarray (CTO NA) was further synthesized via a Co/K ion exchange reaction by the use of KTO NA as a precursor. When applied as electrocatalyst for HER, the binder-free CTO NA exhibits high catalytic activity and superior stability in 0.1 M KOH solution, showing a small overpotential of 199 mV at a current density of 10 mA cm^{-2} and a low Tafel slope of 93 mV dec^{-1}. The catalytic performance enhancement mechanism of CTO NA is proposed. We believe that the layered crystal structure, special chemical composition and three-dimensional hierarchical morphology of the CTO NA are responsible for its outstanding HER catalytic performance.

2. EXPERIMENTAL SECTION

2.1. Synthesis of Potassium Titanate Nanoarray. All reagents were used as received without further purification. Ti foils (0.2 mm in thickness) were degreased by acetone and rinsed with deionized water for several times, followed by drying in N_2 flow. For the synthesis of KTO NA, two pieces of Ti foils (1 × 2 cm^2) were immersed in 8 mL of 10 M KOH solution in a 10 mL sealed glass bottle, and the system was kept at 70 °C for 12 h. Finally, the samples were washed

DOI: 10.1021/acsaem.9b01994
ACS Appl. Energy Mater. 2019, 2, 8946−8955

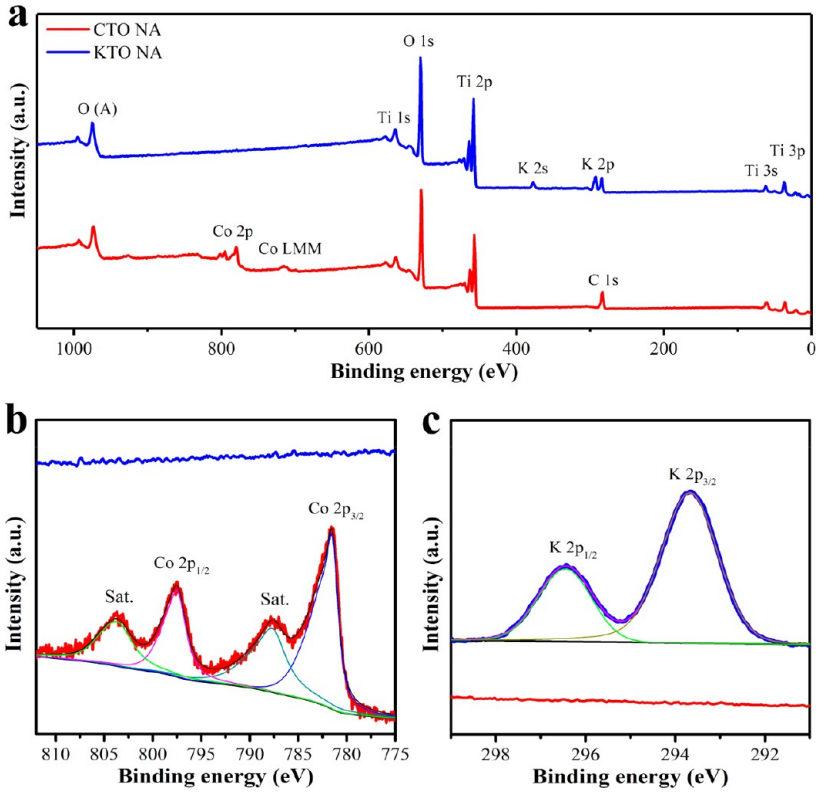

Figure 2. (a) XPS survey spectra, and high-resolution XPS spectra in (b) Co 2p and (c) K 2p regions of KTO NA and CTO NA.

thoroughly with deionized water to remove any remaining KOH. The produced KTO NA was stored in pure water for further uses. The determined loading of KTO NA on Ti foil is 5.0 mg cm^{-2}.

2.2. Synthesis of Cobalt Ion Modified Titanate Nanoarray. CTO NA was prepared via an ion exchange method. Typically, one piece of as-obtained KTO NA was immersed in 8 mL of 1 M $Co(NO_3)_2$ solution in a 10 mL sealed glass bottle, and the Co/K ion exchange reaction was performed at 70 °C in an electric oven for 20 h. After the reaction, CTO NA was washed thoroughly with deionized water and dried in a vacuum oven at 60 °C for 12 h. The determined loading of CTO NA is 4.7 mg cm^{-2}. CTO NA electrocatalysts with various ion exchange durations were prepared at identical experimental procedures except that Co/K ion exchange reaction time was controlled.

2.3. Synthesis of Hydrogen Titanate Nanoarray. Hydrogen titanate nanoarray (HTO NA) was prepared via an H/K ion exchange reaction. For the synthesis of HTO NA, one piece of KTO NA was immersed into 8 mL of 1 M HCl solution in a 10 mL sealed glass bottle, followed by heating to 70 °C for 4 h in an electronic oven to conduct the H/K ion exchange reaction. Finally, HTO NA was washed thoroughly with deionized water and dried in a vacuum oven at 60 °C for 12 h.

2.4. Material Characterization. Powder X-ray diffraction (XRD) data were obtained on a Shimadzu XRD-7000 diffractometer with Cu Kα radiation (λ = 1.5418 Å). Scanning electron microscopy (SEM) and energy dispersive (EDS) X-ray analysis were carried out with a field emission scanning electron microscope (JSM7800F) at an accelerating voltage of 10 kV. Transmission electron microscopy (TEM) measurements were performed by a JEM-2100 electron microscope at an accelerating voltage of 200 kV. X-ray photoelectron spectra (XPS) were examined by an ESCALAB 250Xi X-ray photoelectron spectrometer.

2.5. Electrochemical Characterization. Electrochemical characterizations were performed in a typical three-electrode configuration in 0.1 M KOH electrolyte (pH 13), in which a saturated calomel electrode (SCE) equipped with a salt bridge served as a reference electrode and a graphite plate was used as a counter electrode. All potentials were measured with SCE and converted to reversible hydrogen electrode (RHE) scale via the Nernst equation, $E_{RHE} = E_{SCE} + 0.242 + 0.059pH$ (V).[23] In each measurement, the working electrode was protected with an insulating coating; for precise control only 0.5 × 0.5 cm^2 of the geometric surface area can access the electrolyte. Polarization curves were collected at a scan rate of 2 mV s^{-1}. Durability evaluation by cyclic voltammetry (CV) was performed at a scan rate of 100 mV s^{-1} with a range of −0.3−0.1 V. The $i-t$ curve was recorded under a static overpotential of 200 mV. Electrochemical impedance spectroscopy (EIS) was measured over a frequency range of 0.1−100k Hz under an overpotential of 200 mV with an AC potential amplitude of 5 mV. Owing to the ohmic losses of system resistance, as-measured electrochemical data could not reflect the intrinsic catalytic behaviors of the catalyst. Therefore, all of the electrochemical data were iR corrected before further analysis. The ohmic resistance was determined to be 19.7 Ω according to the real component value of the impedance at the minimum of the Nyquist plot (Figure 7b).[24]

3. RESULTS AND DISCUSSION

KTO NA is in situ grown on Ti foil in a concentrated KOH solution by the use of Ti foil as both reactant and substrate. The XRD pattern of KTO NA that was scraped from the substrate only has two broad peaks at 28.0 and 48.0° due to the low crystallinity nature (Supporting Information Figure S1), which can be sequentially indexed to (310) and (020) planes of $K_2Ti_4O_9$ (JCPDS No. 32-0861).[18] Figure 1a displays that KTO NA exhibits a typical array-like structure, which is very different from that of bare Ti foil with a smooth surface (Figure S2). KTO NA is mainly constructed from nanorods with a diameter of ∼100 nm; meanwhile, some small nanowires are found to interconnect between the nanorods, presenting a reinforced three-dimensional hierarchical structure (Figure 1b). The thickness of the KTO NA layer is determined to be ∼2 μm from the cross-section SEM image

DOI: 10.1021/acsaem.9b01994
ACS Appl. Energy Mater. 2019, 2, 8946−8955

(Figure S3a). The high-resolution TEM image in Figure 1c reveals that KTO NA has a lattice fringe of 0.87 nm which is close to the (200) lattice plane of $K_2Ti_4O_9$ and consistent with the reported data.[25,26] These observations above indicate the successful formation of KTO NA on Ti substrate, in which the determined loading of KTO NA is 5.0 mg cm^{-2}. Cobalt ion modified titanate nanoarray was obtained via a Co/K ion exchange reaction by the use of KTO NA as precursor. After ion exchange treatment, CTO NA inherits the three-dimensional hierarchical structure of KTO NA, but the density of nanorods increases obviously (Figure 1d,e). In addition, the determined loading of CTO NA is 4.7 mg cm^{-2}, lower than that of KTO NA. This is possibly attributed to the loss of CTO NA in solution during the dissolution−recrystallization (Ostwald ripening) process. Figure S3b shows that the layer thickness of CTO NA is about 2 μm, similar to its precursor. In the corresponding XRD pattern, CTO NA shows diffraction peaks similar to that of KTO NA (Figure S1). The high-resolution TEM image in Figure 1f illustrates that CTO NA also has a laminar crystal structure. Its lattice fringe is determined to be 0.74 nm, which is slightly smaller than that of KOT NA. The interlayer distance of the (200) plane of $K_2Ti_4O_9$ is 0.87 nm,[25] and the radius of K^+ is 0.133 nm , which is larger than that of Co^{2+} (0.072 nm).[27] Therefore, the K^+ in KTO could be easily replaced by much smaller sized Co^{2+} and further lead to the shrinking of interlayer spacing.

The surface composition of the materials is analyzed by XPS measurements. Figure 2a shows the survey XPS spectra of KTO NA and CTO NA. One can see that typical peaks for Ti, O, and K are detected in KTO NA, consistent with the chemical composition of $K_2Ti_4O_9$. However, after the ion exchange reaction, the converted CTO NA presents several new peaks around 780 eV associated with Co 2p.[28] Meanwhile, the two peaks at 293.7 and 377.0 eV corresponding to K 2p and K 2s are totally vanished.[29] These results suggest that K^+ in KTO NA are successfully replaced by Co^{2+}. The high-resolution XPS spectra in Co 2p and K 2p regions of KTO NA and CTO NA are recorded for further analysis. The Co 2p region of CTO NA can be deconvoluted into four subpeaks (Figure 2b); the two peaks at 781.5 and 797.6 eV are assigned to the characteristic peaks of Co $2p_{3/2}$ and Co $2p_{1/2}$, respectively. Another two peaks at 786.6 and 802.6 eV are sequentially indexed to the shakeup satellite (Sat.) peaks of Co $2p_{3/2}$ and Co $2p_{1/2}$.[30] As excepted, no signal can be detected in the Co 2p region for the KTO NA (Figure 2b). Moreover, observation of the Co $2p_{3/2}$ peak at 781.5 eV indicates that cobalt in CTO NA presents in +2 oxidation state.[31] In the K 2p region (Figure 2c), two peaks centered at 293.7 and 296.5 eV are observed for KTO NA, which can be well-fitted to the characteristic peaks of K $2p_{3/2}$ and K $2p_{1/2}$,[32] respectively. However, the peaks of K $2p_{3/2}$ and K $2p_{1/2}$ are invisible after converting to CTO NA. EDS spectra of CTO NA, KTO NA, and Ti foil are shown in Figure S4, in which Ti foil only has peaks for metallic titanium. From the spectrum for KTO NA emerges two new peaks at 0.52 and 3.31 K eV, which can be indexed to the Kα peaks of O and K, respectively.[33,34] After converting to CTO NA via an ion exchange reaction, however, the peaks corresponding to K vanish while new peaks of Co Lα (0.78 keV) and Co Kα (6.92 keV) are seen,[35] further confirming that K^+ in KTO NA is replaced by Co^{2+}. The EDS results are in good agreement with those of the XPS measurements.

The electrocatalytic activity of CTO NA and KTO NA toward HER was examined in 0.1 M KOH electrolyte with a typical three-electrode configuration. The catalytic behaviors of Pt/C (20%) and bare Ti foil are also studied as reference. Figure 3a shows the *iR* corrected polarization curves of CTO

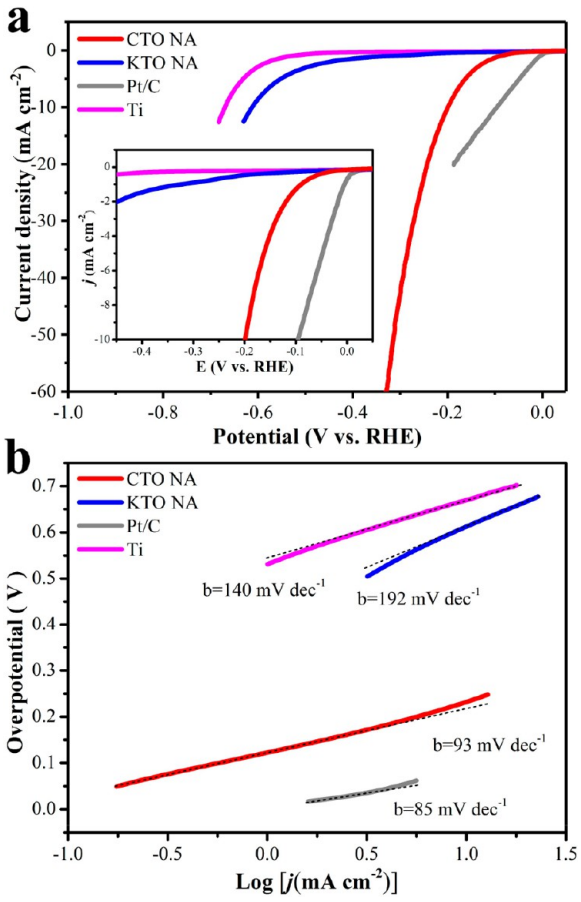

Figure 3. (a) Polarization curves and (b) Tafel plots of CTO NA, KTO NA, Ti foil, and Pt/C.

NA, KTO NA, bare Ti foil, and Pt/C. One can see that Pt/C catalyst displays an outstanding catalytic activity toward HER with an onset overpotential near 0 mV. In sharp contrast, only very weak HER current densities can be observed at high-overpotential range for both KTO NA and Ti foil, suggesting their poor catalytic activity. However, the CTO NA catalyst shows a low onset potential of ~30 mV for HER, and its catalytic current increases dramatically when the potential turns slightly negative (inset of Figure 3a), signifying the high catalytic activity. In addition, the CTO NA catalyst only needs a small overpotential of 199 mV at a current density of 10 mA cm^{-2}, much lower than that of KTO NA (613 mV) and Ti foil (670 mV), further confirming the superior HER catalytic activity of CTO NA. In terms of the overpotential at 10 mA cm^{-2}, the catalytic performance achieved by CTO NA catalyst outperforms most reported non-noble metal HER catalysts under identical conditions, such as C_{60}-SWCNT$_{15}$ (380),[36] WC@CNS (220 mV),[37] Mn_1Ni_1 (360 mV),[38] 1D N-Mo_2C (239 mV),[39] $NiMo_3S_4$ (257 mV),[40] $NiMoS_4$/Ti (194 mV),[41] Co@NC (277 mV),[42] 2D i-WC-G 70% (~225 mV),[43] and Cu_3P/CF(222 mV),[44] etc.

Figure 3b shows the Tafel plots of CTO NA, KTO NA, Ti foil, and Pt/C. The linear portions of the curves are fitted to

DOI: 10.1021/acsaem.9b01994
ACS Appl. Energy Mater. 2019, 2, 8946−8955

the Tafel equation. The Pt/C catalyst exhibits a Tafel slope of 85 mV dec^{-1}, which is lower than the reported value (113 dec^{-1}) under identical operating condition.[45] However, both KTO NA and Ti foil exhibit much higher Tafel slopes of 192 and 140 mV dec^{-1}, respectively. Remarkably, the CTO NA catalyst shows a small Tafel slope of 93 mV dec^{-1}, which is only 8 mV dec^{-1} difference from Pt/C and a half of that for KTO NA. The lower Tafel slope of CTO NA indicates that it has much more favorable electrode kinetics toward HER than that of KTO NA and bare Ti foil. It is worth noting that the Tafel slope achieved by CTO NA is lower than many reported non-noble metal HER catalysts under the same operating conditions, including C_{60}-SWCNT$_{15}$ (121 mV dec^{-1}),[38] $NiMo_3S_4$ (98 mV dec^{-1}),[40] $NiMoS_4$/Ti (97 mV dec^{-1}),[41] Cu_3P/CF (148 mV dec^{-1}),[44] np-CuTi (110 mV dec^{-1}),[46] NiCoMo (108 mV dec^{-1}),[47] Bi-NP Cu/Al_7Cu_4Ni@Cu_4Ni (~110 mV dec^{-1}),[48] and MoN_x/Ni-foam (121 mV dec^{-1}),[49] etc. In order to further understand the enhancement mechanism for the produced catalytic activity, exchange current density (i_0) is calculated from the Tafel plot according to the reported method.[50] As shown in Figure S5, Pt/C exhibits an i_0 of 0.76 mA cm^{-2}, which is very close to the previously reported data (0.63 mA cm^{-2}).[45] Amazingly, as a non-noble metal material, the CTO NA catalyst has an i_0 of 5.6 × 10^{-2} mA cm^{-2}; although the value is inferior to the Pt/C benchmark HER catalyst, it is still distinctly higher than that of KTO NA (3.9 × 10^{-3} mA cm^{-2}) and Ti foil (7.1 × 10^{-5} mA cm^{-2}). This result indicates that the CTO NA catalyst has higher intrinsic HER catalytic activity than KTO NA and Ti foil.

To further understand the catalytic behaviors, the CTO NA catalysts with different ion exchange durations were synthesized and investigated in identical conditions. Figure 4a shows that the polarization curves shift to the right direction as the ion exchange time increases, indicating the HER catalytic activity is enhanced gradually. The overpotentials of the CTO NA catalysts at a current density of 10 mA cm^{-2} are extracted for further analysis (Figure 4b). One can see that the overpotential decreases obviously when prolonging the ion exchange time and attaining the lowest value at 20 h. Further increasing the reaction time leads to a rise of the overpotential, which is probably attributed to the dissolution−recrystallization (Ostwald ripening) process for a reduced surface area.[51] In a solution, Ostwald ripening is a spontaneous phenomenon using surface energy reduction as a driving force.[52,53] This process leads to dissolution of small-sized crystals whose surface energy is high while forming larger ones with reduced surface area.[53] SEM images of CTO NA catalysts synthesized at ion exchange times of 0, 4, 8, 12, 16, 20, 24, and 28 h are shown in Figure 5. Before the reaction period of 20 h, increasing the ion exchange time results in a reduced number of connected nanowires; meanwhile the density of nanorods is increased (Figure 5a−f). Further extending the ion exchange time leads to the aggregation of the nanoarray (Figure 5g,h), which is a consequence of the Ostwald ripening. This obviously reduces the surface area of CTO NA and lowers the catalytic performance. To understand the chemical composition variation during the ion exchange, as-synthesized CTO NA catalysts were analyzed by EDS measurements. As shown in Figure S6, prominent signals for Co are detected in the catalysts prepared at ion exchange times of 4, 8, 12, 16, and 20 h, while the K signals totally disappear until the ion exchange peroid attains 20 h. These results suggest that a

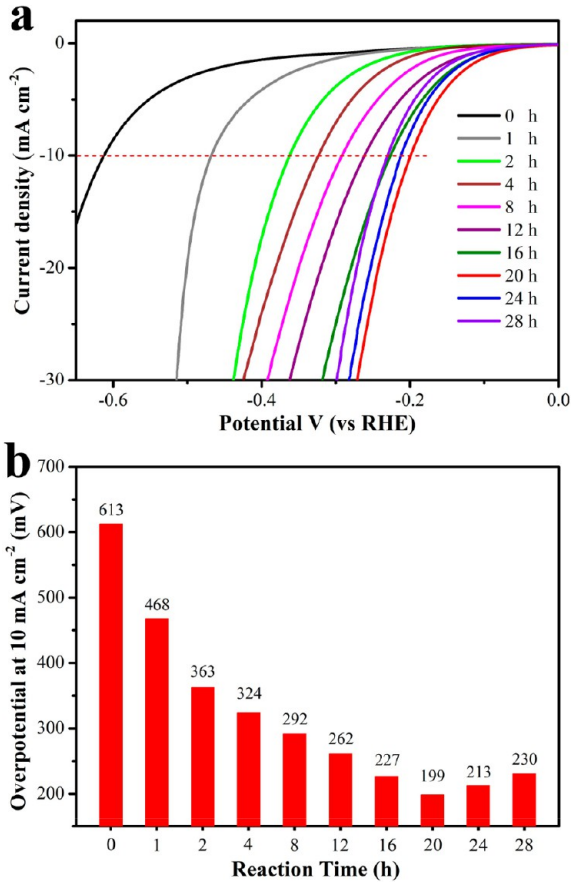

Figure 4. (a) Polarization curves and (b) overpotentials at 10 mA cm^{-2} of CTO NA catalysts synthesized at different ion exchange durations.

duration of 20 h is necessary to complete Co/K ion exchange reaction. As shown in Figure S7a, the Nyquist plots of the CTO NA catalysts acquired under a static overpotential of 200 mV have well-defined semicircles, of which the diameter corresponds to the charge transfer resistance (R_{ct}) in electrochemical reactions.[54] The R_{ct} of CTO NA catalysts decreases dramatically with raising the ion exchange time (Figure S7a,b), vividly symbolizing that the electrode kinetics is remarkably enhanced. The ion exchange time dependent catalytic behaviors of CTO NA probably controlled by the amount of K^+ in KTO replaced by Co^{2+}.

Stability is an important parameter of an electrocatalyst in practical applications; thus, the long-term operating stability of CTO NA catalyst is studied, and the results are shown in Figure 6. After continuous 3000 CV cycles over a range of −0.3−0.1 V at a scan rate of 100 mV s^{-1}, the polarization curve exhibits the same features as the initial one without obvious loss of current density (Figure 6a), indicating the decay of catalytic activity is negligible after the cycling. Figure 6b shows the i−t curve of CTO NA acquired at a constant overpotential of 200 mV. It can be seen that the electrocatalytic activity of CTO NA toward HER maintains at least 20 h. It is worthy of note that after the i−t test, CTO NA still keeps the original three-dimensional hierarchical morphology, and the nanoarray is well-preserved (Figure S8). Snice CTO NA was prepared via a Co/K ion exchange reaction by the use of KTO as precursor, therefore, there is a possibility that Co^{2+} in CTO NA is reversibly exchanged by K^+ in KOH solution. Nevertheless, we

DOI: 10.1021/acsaem.9b01994
ACS Appl. Energy Mater. 2019, 2, 8946−8955

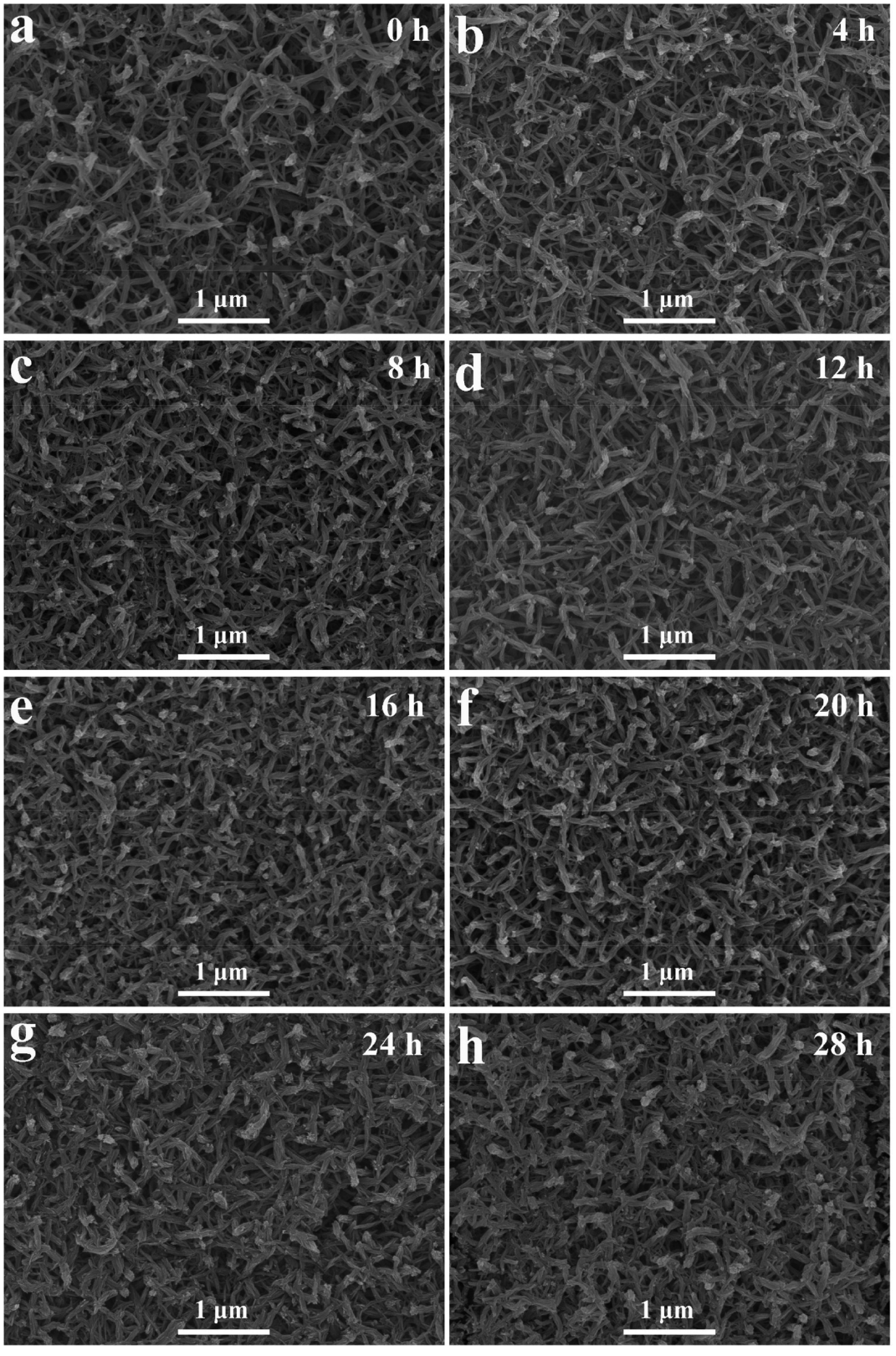

Figure 5. SEM images of CTO NA catalysts synthesized at different ion exchange durations.

believe that the reexchange of Co^{2+} in CTO NA is negligible when operating in 0.1 M KOH electrolyte, this is because the leached cobalt ions tend to in situ generate $Co(OH)_2$ and attach on CTO NA to impede further loss of Co^{2+}. This hypothesis is supported by chemical composition analysis via XPS measurements. As shown in Figure S9, there is no K signal existing in the survey XPS spectrum of CTO NA recorded after the *i*−t test, suggesting its chemical composition remains unchanged during long-term HER process. These results demonstrate that CTO NA has a strong capability to resist the

DOI: 10.1021/acsaem.9b01994
ACS Appl. Energy Mater. 2019, 2, 8946−8955

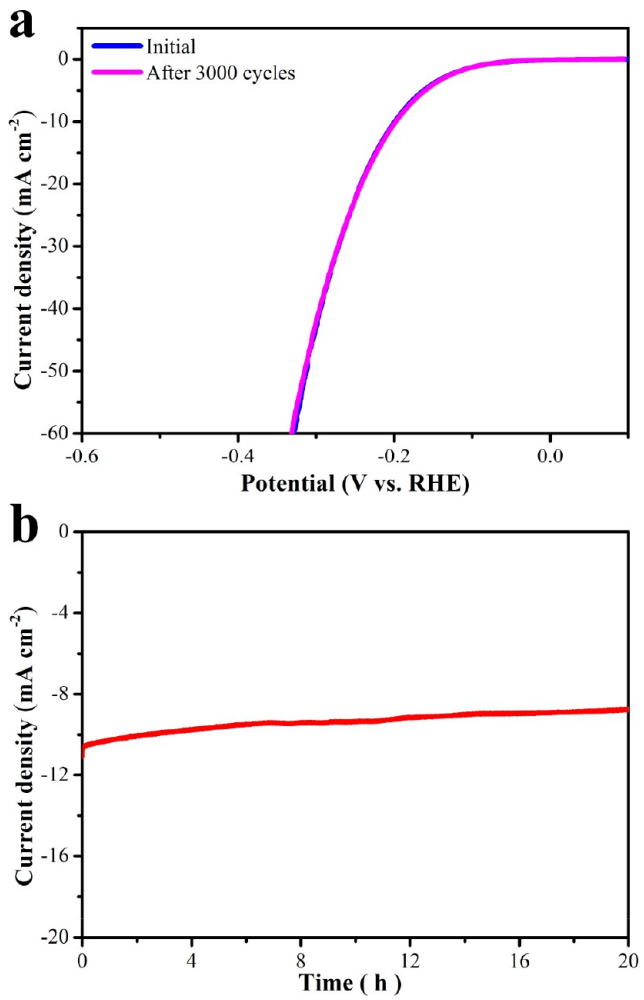

Figure 6. (a) Polarization curves of CTO NA recorded initially and after 3000 CV cycles, (b) *i*−t curve of CTO NA achieved under a static overpotential of 200 mV.

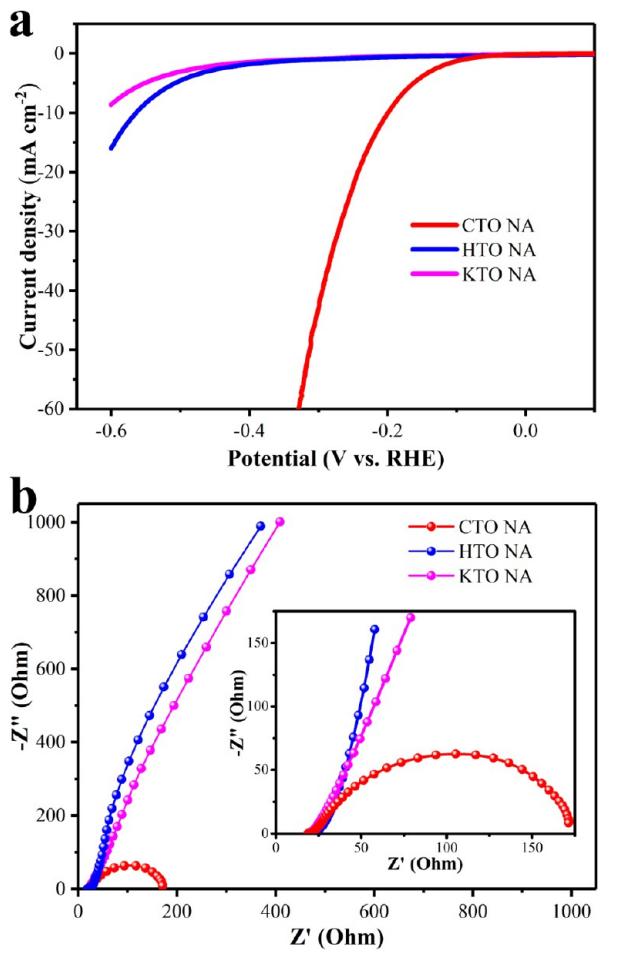

Figure 7. (a) Polarization curves and (b) Nyquist plots of CTO NA, HTO NA, and KTO NA.

chemical/electrochemical corrosions in 0.1 M KOH solution for an extraordinary long-term operating stability toward HER, which is a benefit for practical applications.

To understand the catalytic mechanism, hydrogen titanate nanoarray was prepared via an H/K ion exchange reaction.[17] Panels a and b of Figure S10 reveal that HTO NA also has an array-like morphology, similar to its precursor. In the corresponding EDS measurement (Figure S11), the signal for K element is invisible, evidencing that the K^+ in the KTO is replaced by proton. The polarization curve of HTO NA is illustrated in Figure 7a, which shows poor HER catalytic activity. HTO NA exhibits a high overpotential of 564 mV at a current density of 10 mA cm^{-2}, a Tafel of 181 mV dec^{-1}, and an i_0 of 7.8 × 10^{-3} mA cm^{-2} (Figure S12a,b), which are inferior to those of CTO NA. For better comparison, the polarization curves of CTO NA and KTO NA are also presented in Figure 7a. Both KTO NA and HTO NA are inactive toward HER; only small HER current densities are observed when the overpotential is higher than 400 mV, while the CTO NA catalyst is highly active. The Nyquist plots in Figure 7b reveal that CTO NA catalyst has a smaller semicircle than those of KTO NA and HTO NA, indicating the CTO NA possesses lower R_{ct} for the fastest charge transfer in HER. The results discussed above demonstrate that the CTO NA catalyst is kinetically much more active toward HER than KTO NA and HTO NA. The significant discrepancies in catalytic acvitity are likely to relate to their different crystal structures, and we argue that the cobalt ion in CTO NA is the catalytic active sites for HER.

The overall preparation procedures and crystal structures of CTO NA, KTO NA, and HTO NA are schematically illustrated in Figure 8. In KTO NA, one layer of positively charged K^+ distributes between two layers of negatively charged TiO_6 octahedron, and K^+ could be replaced by Co^{2+}/H^+ to generate CTO NA and HTO NA. Since Co^{2+} in CTO NA has unoccupied 3d orbitals, the electrons from the conductive substrate could easily access to the orbitals during the electrochemical reactions.[55] Owing to the Co^{2+} in CTO NA being distributed in a plane, the electrons could transfer from one to another via the unoccupied 3d orbitals through the plane for a high electron transfer rate to promote hydrogen evolution. Nevertheless, both K and H ions in corresponding titanates have no unoccupied valence electron orbit to accept any external electron, which would suppress the electron transfer process to hinder the HER. This conclusion is supported by the Nyquist plots (Figure 7b) analysis as discussed above. Therefore, the layered crystal structure and unique chemical composition of CTO NA is primarily responsible for its outstanding HER catalytic activity. In addition, the mass transport and charge transfer of the CTO NA in HER are greatly enhanced by its three-dimensional hierarchical morphology. For example, the channels and voids

DOI: 10.1021/acsaem.9b01994
ACS Appl. Energy Mater. 2019, 2, 8946−8955

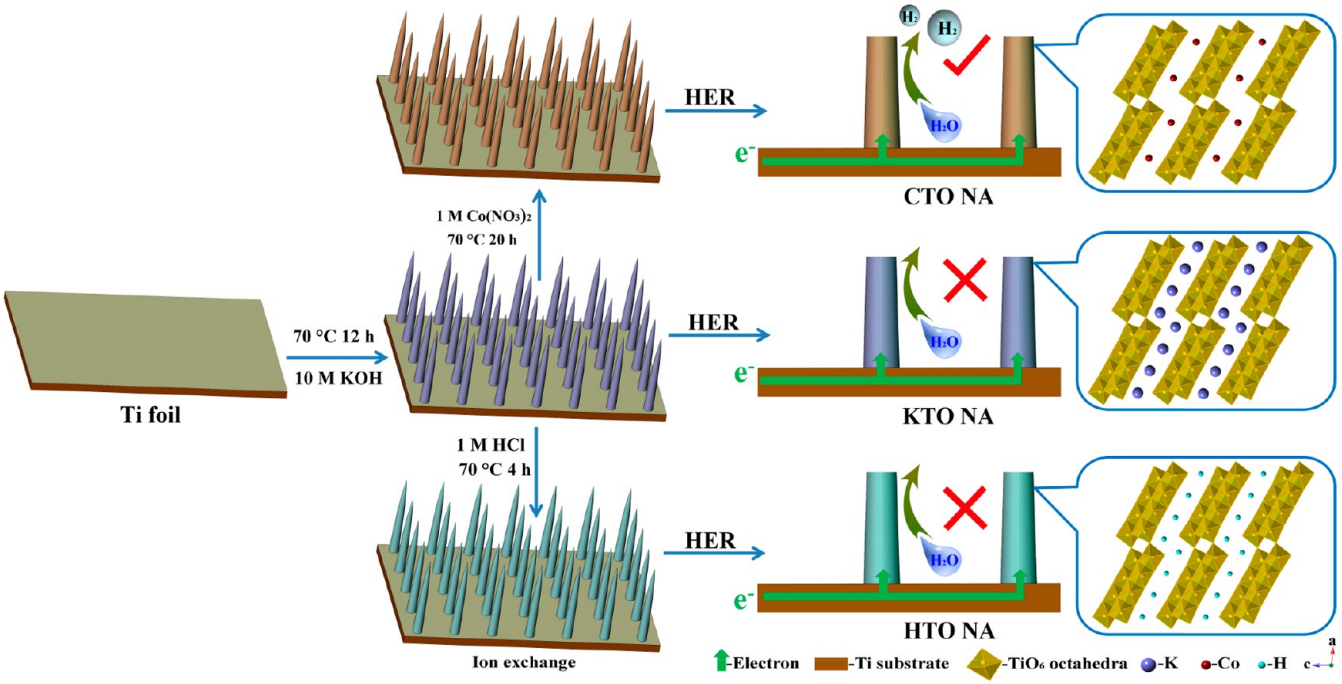

Figure 8. Illustration of material synthesis and HER catalytic mechanisms of CTO NA, KTO NA, and HTO NA.

between the nanorods could serve as paths allowing the fast escape of the produced hydrogen bubbles to enhance the mass transport; the CTO NA catalyst comprising nanorods interconnecting with small nanowires can not only enhance charge transfer but also aggressively improve the stability by a reinforced structure. Moreover, the binder-free nature of CTO NA guarantees the catalyst could expose more active sites to the electrolyte, thus endowing high catalytic activity. In a brief, the above factors jointly contribute to the superior catalytic activity and stability of CTO NA toward HER.

4. CONCLUSIONS

In summary, CTO NA has successfully synthesized as a high-performance electrocatalyst for HER via a facile ion exchange process. This binder-free catalyst with a unique three-dimensional hierarchical structure exhibits excellent catalytic activity and durability toward HER in 0.1 M KOH electrolyte, showing a small Tafel slope of 93 mV dec^{-1} and a low overpotential of 199 mV at a current density of 10 mA cm^{-2}, which outperform those of most reported HER catalysts under the same operating conditions. According to the experimental results, the superior catalytic activity of CTO NA could mainly be ascribed to its layered crystal structure and unique chemical composition as well as three-dimensional hierarchical morphology. This work not only holds great promise to the as-prepared non-noble metal material as an alternative for the noble metals based catalysts toward HER but also sheds scientific light on a way to tailor a catalyst from both physics and chemistry for synergistically enhancing catalytic activity.

■ ASSOCIATED CONTENT

Supporting Information

The Supporting Information is available free of charge at https://pubs.acs.org/doi/10.1021/acsaem.9b01994.

XRD patterns, SEM images, EDS and XPS spectra, exchange current densities, Nyquist plots, and Tafel plot (PDF)

■ AUTHOR INFORMATION

Corresponding Authors

*(C.M.L.) E-mail: ecmli@swu.edu.cn.
*(T.Y.) E-mail: yuting@ntu.edu.sg.

ORCID

Hongfang Du: 0000-0002-2673-4008
Lian Ying Zhang: 0000-0002-2281-6794
Yubin Niu: 0000-0002-1458-7469
Ting Yu: 0000-0001-5782-1588
Chang Ming Li: 0000-0002-4041-2574

Notes

The authors declare no competing financial interest.

■ ACKNOWLEDGMENTS

This work was financially supported by the Institute for Clean Energy & Advanced Materials (Southwest University, Chongqing, China); Ministry of Education (MOE) Tier 1 (RG19/17); the Start-up grant under SWU111071 from the Southwest University (Chongqing, China); and the Graduate Student Research Innovation Project of Chongqing (Grant No. CYB16055).

■ REFERENCES

(1) Voiry, D.; Shin, H. S.; Loh, K. P.; Chhowalla, M. Low-dimensional Catalysts for Hydrogen Evolution and CO_2 Reduction. *Nat. Rev. Chem.* **2018**, *2*, 0105.

(2) Pu, Z.; Zhao, J.; Amiinu, I. S.; Li, W.; Wang, M.; He, D.; Mu, S. A Universal Synthesis Strategy for P-rich Noble Metal Diphosphide-based Electrocatalysts for the Hydrogen Evolution Reaction. *Energy Environ. Sci.* **2019**, *12*, 952−957.

(3) Yin, B.; Cao, X.; Pan, A.; Luo, Z.; Dinesh, S.; Lin, J.; Tang, Y.; Liang, S.; Cao, G. Encapsulation of CoS_x Nanocrystals into N/S Co-

DOI: 10.1021/acsaem.9b01994
ACS Appl. Energy Mater. 2019, 2, 8946−8955

Doped Honeycomb-like 3D Porous Carbon for High-performance Lithium Storage. *Adv. Sci.* **2018**, *5*, 1800829.
(4) Wang, Y.; Pan, A.; Zhang, Y.; Shi, J.; Lin, J.; Liang, S.; Cao, G. Heterogeneous NiS/NiO Multi-shelled Hollow Microspheres with Enhanced Electrochemical Performances for Hybrid-type Asymmetric Supercapacitors. *J. Mater. Chem. A* **2018**, *6*, 9153−9160.
(5) Huang, Y.; Sun, Y.; Zheng, X.; Aoki, T.; Pattengale, B.; Huang, J.; He, X.; Bian, W.; Younan, S.; Williams, N.; Hu, J.; Ge, J.; Pu, N.; Yan, X.; Pan, X.; Zhang, L.; Wei, Y.; Gu, J. Atomically Engineering Activation Sites onto Metallic 1T-MoS_2 Catalysts for Enhanced Electrochemical Hydrogen Evolution. *Nat. Commun.* **2019**, *10*, 982.
(6) Zhang, Y.; Su, Q.; Xu, W.; Cao, G.; Wang, Y.; Pan, A.; Liang, S. A Confined Replacement Synthesis of Bismuth Nanodots in MOF Derived Carbon Arrays as Binder-free Anodes for Sodium-ion Batteries. *Adv. Sci.* **2019**, *6*, 1900162.
(7) Zheng, Y.; Jiao, Y.; Vasileff, A.; Qiao, S.-Z. The Hydrogen Evolution Reaction in Alkaline Solution: From Theory, Single Crystal Models, to Practical Electrocatalysts. *Angew. Chem., Int. Ed.* **2018**, *57*, 7568−7579.
(8) Du, H.; Ai, W.; Zhao, Z. L.; Chen, Y.; Xu, X.; Zou, C.; Wu, L.; Su, L.; Nan, K.; Yu, T.; Li, C. M. Engineering Morphologies of Cobalt Pyrophosphates Nanostructures toward Greatly Enhanced Electrocatalytic Performance of Oxygen Evolution Reaction. *Small* **2018**, *14*, 1801068.
(9) Nairan, A.; Zou, P.; Liang, C.; Liu, J.; Wu, D.; Liu, P.; Yang, C. NiMo Solid Solution Nanowire Array Electrodes for Highly Efficient Hydrogen Evolution Reaction. *Adv. Funct. Mater.* **2019**, *29*, 1903747.
(10) Hu, Y.; Yang, H.; Chen, J.; Xiong, T.; Balogun, M. S. J. T.; Tong, Y. Efficient Hydrogen Evolution Activity and Overall Water Splitting of Metallic Co_4N Nanowires through Tunable d-orbitals with Ultrafast Incorporation of FeOOH. *ACS Appl. Mater. Interfaces* **2019**, *11*, 5152−5158.
(11) Hu, C.; Dai, L. Multifunctional Carbon-based Metal-free Electrocatalysts for Simultaneous Oxygen Reduction, Oxygen Evolution, and Hydrogen Evolution. *Adv. Mater.* **2017**, *29*, 1604942.
(12) Du, H.; Gu, S.; Liu, R.; Li, C. M. Tungsten Diphosphide Nanorods as an Efficient Catalyst for Electrochemical Hydrogen Evolution. *J. Power Sources* **2015**, *278*, 540−545.
(13) Chen, Z.; Duan, X.; Wei, W.; Wang, S.; Ni, B.-J. Recent Advances in Transition Metal-based Electrocatalysts for Alkaline Hydrogen Evolution. *J. Mater. Chem. A* **2019**, *7*, 14971−15005.
(14) Zhang, L.; Zhang, Q.; Li, J. Layered Titanate Nanosheets Intercalated with Myoglobin for Direct Electrochemistry. *Adv. Funct. Mater.* **2007**, *17*, 1958−1965.
(15) Liu, J.; Tang, S.; Lu, Y.; Cai, G.; Liang, S.; Wang, W.; Chen, X. Synthesis of Mo_2N Nanolayer Coated MoO_2 Hollow Nanostructures as High-Performance Anode Materials for Lithium-ion Batteries. *Energy Environ. Sci.* **2013**, *6*, 2691−2697.
(16) Izawa, H.; Kikkawa, S.; Koizumi, M. Ion Exchange and Dehydration of Layered [Sodium and Potassium] Titanates, $Na_2Ti_3O_7$ and $K_2Ti_4O_9$. *J. Phys. Chem.* **1982**, *86*, 5023−5026.
(17) Zhu, H. Y.; Lan, Y.; Gao, X.; Ringer, S. P.; Zheng, Z.; Song, D. Y.; Zhao, J.-C. Phase Transition Between Nanostructures of Titanate and Titanium Dioxides via Simple Wet-chemical Reactions. *J. Am. Chem. Soc.* **2005**, *127*, 6730−6736.
(18) Zhou, W.; Liu, X.; Sang, Y.; Zhao, Z.; Zhou, K.; Liu, H.; Chen, S. Enhanced Performance of Layered Titanate Nanowire-based Supercapacitor Electrodes by Nickel Ion Exchange. *ACS Appl. Mater. Interfaces* **2014**, *6*, 4578−4586.
(19) Sasaki, T.; Izumi, F.; Watanabe, M. Intercalation of Pyridine in Layered Titanates. *Chem. Mater.* **1996**, *8*, 777−782.
(20) Yang, D.; Zheng, Z.; Liu, H.; Zhu, H.; Ke, X.; Xu, Y.; Wu, D.; Sun, Y. Layered Titanate Nanofibers as Efficient Adsorbents for Removal of Toxic Radioactive and Heavy Metal Ions from Water. *J. Phys. Chem. C* **2008**, *112*, 16275−16280.
(21) Kishore, B.; G, V.; Munichandraiah, N. $K_2Ti_4O_9$: A Promising Anode Material for Potassium Ion Batteries. *J. Electrochem. Soc.* **2016**, *163*, A2551−A2554.
(22) Liu, H.; Lin, B.; He, L.; Qu, H.; Sun, P.; Gao, B.; Chen, Y. Mesoporous Cobalt-intercalated Layered Tetratitanate for Efficient Visible-light Photocatalysis. *Chem. Eng. J.* **2013**, *215*−*216*, 396−403.
(23) Peng, X.; Qasim, A. M.; Jin, W.; Wang, L.; Hu, L.; Miao, Y.; Li, W.; Li, Y.; Liu, Z.; Huo, K.; Wong, K.-y.; Chu, P. K. Ni-doped Amorphous Iron Phosphide Nanoparticles on TiN Nanowire Arrays: an Advanced Alkaline Hydrogen Evolution Electrocatalyst. *Nano Energy* **2018**, *53*, 66−73.
(24) van der Vliet, D.; Strmcnik, D. S.; Wang, C.; Stamenkovic, V. R.; Markovic, N. M.; Koper, M. T. M. On the Importance of Correcting for the Uncompensated Ohmic Resistance in Model Experiments of the Oxygen Reduction Reaction. *J. Electroanal. Chem.* **2010**, *647*, 29−34.
(25) Melo, M. A.; Carminati, S. A.; Bettini, J.; Nogueira, A. F. Pillaring and NiO_x Co-catalyst Loading as Alternatives for the Photoactivity Enhancement of $K_2Ti_4O_9$ towards Water Splitting. *Sustainable Energy Fuels* **2018**, *2*, 958−967.
(26) Amano, F.; Yasumoto, T.; Shibayama, T.; Uchida, S.; Ohtani, B. Nanowire-structured Titanate with Anatase Titania: Characterization and Photocatalytic Activity. *Appl. Catal., B* **2009**, *89*, 583−589.
(27) Ahrens, L. H. The Use of Ionization Potentials Part 1. Ionic Radii of the Elements. *Geochim. Cosmochim. Acta* **1952**, *2*, 155−169.
(28) Gupta, S.; Patel, N.; Fernandes, R.; Kadrekar, R.; Dashora, A.; Yadav, A. K.; Bhattacharyya, D.; Jha, S. N.; Miotello, A.; Kothari, D. C. Co−Ni−B Nanocatalyst for Efficient Hydrogen Evolution Reaction in wide pH Range. *Appl. Catal., B* **2016**, *192*, 126−133.
(29) Song, W.; Tian, M.; Chen, F.; Tian, Y.; Wan, C.; Yu, X. The Study on the Degradation and Mineralization Mechanism of Ion-doped Calcium Polyphosphate in Vitro. *J. Biomed. Mater. Res., Part B* **2009**, *89B*, 430−438.
(30) Verma, S.; Kumar, A.; Pravarthana, D.; Deshpande, A.; Ogale, S. B.; Yusuf, S. M. Off-stoichiometric Nickel Cobaltite Nanoparticles: Thermal Stability, Magnetization, and Neutron Diffraction Studies. *J. Phys. Chem. C* **2014**, *118*, 16246−16254.
(31) Xiang, J.; Wen, X.; Zhang, F. Supported Nickel−cobalt Bimetallic Catalysts Derived from Layered Double Hydroxide Precursors for Selective Hydrogenation of Pyrolysis Gasoline. *Ind. Eng. Chem. Res.* **2014**, *53*, 15600−15610.
(32) Štengl, V.; Henych, J.; Szatmáry, L.; Kormunda, M. Photocatalytic Oxidation of Butane by Titania after Reductive Annealing. *J. Mater. Sci.* **2014**, *49*, 4161−4170.
(33) Zhang, J.; Fu, J.; Tan, G.; Li, F.; Luo, C.; Zhao, J.; Xie, E.; Xue, D.; Zhang, H.; Mellors, N. J.; Peng, Y. Nanoscale Characterization and Magnetic Reversal Mechanism Investigation of Electrospun $NiFe_2O_4$ Multi-Particle-Chain Nanofibres. *Nanoscale* **2012**, *4*, 2754−2759.
(34) Bueno Guerra, M. B.; Schaefer, C. E.; de Carvalho, G. G.; de Souza, P. F.; Júnior, D. S.; Nunes, L. C.; Krug, F. J. Evaluation of Micro-energy Dispersive X-ray Fluorescence Spectrometry for the Analysis of Plant Materials. *J. Anal. At. Spectrom.* **2013**, *28*, 1096−1101.
(35) Barreca, D.; Fornasiero, P.; Gasparotto, A.; Gombac, V.; Maccato, C.; Pozza, A.; Tondello, E. CVD Co_3O_4 Nanopyramids: a Nano-platform for Photo-assisted H_2 Production. *Chem. Vap. Deposition* **2010**, *16*, 296−300.
(36) Gao, R.; Dai, Q.; Du, F.; Yan, D.; Dai, L. C_{60}-adsorbed Single-walled Carbon Nanotubes as Metal-free, pH-universal, and Multifunctional Catalysts for Oxygen Reduction, Oxygen Evolution, and Hydrogen Evolution. *J. Am. Chem. Soc.* **2019**, *141*, 11658−11666.
(37) Zhu, J.; Sakaushi, K.; Clavel, G.; Shalom, M.; Antonietti, M.; Fellinger, T.-P. A General Salt-templating Method to Fabricate Vertically Aligned Graphitic Carbon Nanosheets and Their Metal Carbide Hybrids for Superior Lithium Ion Batteries and Water Splitting. *J. Am. Chem. Soc.* **2015**, *137*, 5480−5485.
(38) Ledendecker, M.; Clavel, G.; Antonietti, M.; Shalom, M. Highly Porous Materials as Tunable Electrocatalysts for the Hydrogen and Oxygen Evolution Reaction. *Adv. Funct. Mater.* **2015**, *25*, 393−399.

DOI: 10.1021/acsaem.9b01994
ACS Appl. Energy Mater. 2019, 2, 8946−8955

(39) Wan, J.; Wu, J.; Gao, X.; Li, T.; Hu, Z.; Yu, H.; Huang, L. Structure Confined Porous Mo_2C for Efficient Hydrogen Evolution. *Adv. Funct. Mater.* **2017**, *27*, 1703933.
(40) Jiang, J.; Gao, M.; Sheng, W.; Yan, Y. Hollow Chevrel-phase $NiMo_3S_4$ for Hydrogen Evolution in Alkaline Electrolytes. *Angew. Chem., Int. Ed.* **2016**, *55*, 15240−15245.
(41) Wang, W.; Yang, L.; Qu, F.; Liu, Z.; Du, G.; Asiri, A. M.; Yao, Y.; Chen, L.; Sun, X. A self-supported $NiMoS_4$ Nanoarray as an Efficient 3D Cathode for the Alkaline Hydrogen Evolution Reaction. *J. Mater. Chem. A* **2017**, *5*, 16585−16589.
(42) Kuang, M.; Wang, Q.; Han, P.; Zheng, G. Cu,Co-embedded N-enriched Mesoporous Carbon for Efficient Oxygen Reduction and Hydrogen Evolution Reactions. *Adv. Energy Mater.* **2017**, *7*, 1700193.
(43) Zeng, M.; Chen, Y.; Li, J.; Xue, H.; Mendes, R. G.; Liu, J.; Zhang, T.; Rümmeli, M. H.; Fu, L. 2D WC Single Crystal Embedded in Graphene for Enhancing Hydrogen Evolution Reaction. *Nano Energy* **2017**, *33*, 356−362.
(44) Hou, C.-C.; Chen, Q.-Q.; Wang, C.-J.; Liang, F.; Lin, Z.; Fu, W.-F.; Chen, Y. Self-supported Cedarlike Semimetallic Cu_3P Nanoarrays as a 3D High-performance Janus Electrode for Both Oxygen and Hydrogen Evolution under Basic Conditions. *ACS Appl. Mater. Interfaces* **2016**, *8*, 23037−23048.
(45) Sheng, W.; Myint, M.; Chen, J. G.; Yan, Y. Correlating the Hydrogen Evolution Reaction Activity in Alkaline Electrolytes with the Hydrogen Binding Energy on Monometallic Surfaces. *Energy Environ. Sci.* **2013**, *6*, 1509−1512.
(46) Lu, Q.; Hutchings, G. S.; Yu, W.; Zhou, Y.; Forest, R. V.; Tao, R.; Rosen, J.; Yonemoto, B. T.; Cao, Z.; Zheng, H.; Xiao, J. Q.; Jiao, F.; Chen, J. G. Highly Porous Non-precious Bimetallic Electrocatalysts for Efficient Hydrogen Evolution. *Nat. Commun.* **2015**, *6*, 6567.
(47) Gao, D.; Guo, J.; Cui, X.; Yang, L.; Yang, Y.; He, H.; Xiao, P.; Zhang, Y. Three-dimensional Dendritic Structures of NiCoMo as Efficient Electrocatalysts for the Hydrogen Evolution Reaction. *ACS Appl. Mater. Interfaces* **2017**, *9*, 22420−22431.
(48) Sun, J. S.; Wen, Z.; Han, L. P.; Chen, Z. W.; Lang, X. Y.; Jiang, Q. Nonprecious Intermetallic Al_7Cu_4Ni Nanocrystals Seamlessly Integrated in Freestanding Bimodal Nanoporous Copper for Efficient Hydrogen Evolution Catalysis. *Adv. Funct. Mater.* **2018**, *28*, 1706127.
(49) Ramesh, R.; Nandi, D. K.; Kim, T. H.; Cheon, T.; Oh, J.; Kim, S.-H. Atomic-layer-deposited MoN_x Thin Films on Three-dimensional Ni Foam as Efficient Catalysts for the Electrochemical Hydrogen Evolution Reaction. *ACS Appl. Mater. Interfaces* **2019**, *11*, 17321−17332.
(50) Kibsgaard, J.; Chen, Z.; Reinecke, B. N.; Jaramillo, T. F. Engineering the Surface Structure of MoS_2 to Preferentially Expose Active Edge Sites for Electrocatalysis. *Nat. Mater.* **2012**, *11*, 963−969.
(51) Yu, J.; Wang, G.; Cheng, B.; Zhou, M. Effects of Hydrothermal Temperature and Time on The Photocatalytic Activity and Microstructures of Bimodal Mesoporous TiO_2 Powders. *Appl. Catal., B* **2007**, *69*, 171−180.
(52) Luo, Y.-S.; Dai, X.-J.; Zhang, W.-D.; Yang, Y.; Sun, C. Q.; Fu, S.-Y. Controllable Synthesis and Luminescent Properties of Novel Erythrocyte-like $CaMoO_4$ Hierarchical Nanostructures via a Simple Surfactant-free Hydrothermal Route. *Dalton Trans.* **2010**, *39*, 2226−2231.
(53) Li, G.; Guan, L.; Liu, Y.; Liu, C. Template-free Solvothermal Synthesis of 3D Hierarchical Nanostructured Boehmite Assembled by Nanosheets. *J. Phys. Chem. Solids* **2012**, *73*, 1055−1060.
(54) Guo, C. X.; Zhang, L. Y.; Miao, J.; Zhang, J.; Li, C. M. DNA-functionalized Graphene to Guide Growth of Highly Active Pd Nanocrystals as Efficient Electrocatalyst for Direct Formic Acid Fuel Cells. *Adv. Energy Mater.* **2013**, *3*, 167−171.
(55) Qiao, L.; Xiao, H. Y.; Meyer, H.; Sun, J.; Rouleau, C. M.; Puretzky, A. A.; Geohegan, D. B.; Ivanov, I. N.; Yoon, M.; Weber, W. J.; Biegalski, M. D. Nature of the Band Gap and Origin of the Electro-/photo-activity of Co_3O_4. *J. Mater. Chem. C* **2013**, *1*, 4628−4633.

DOI: 10.1021/acsaem.9b01994
ACS Appl. Energy Mater. 2019, 2, 8946−8955